Noname manuscript No.
(will be inserted by the editor)

A Reduced Iwan Model That Includes Pinning for Bolted Joint Mechanics

M. R. W. Brake

the date of receipt and acceptance should be inserted later

Abstract Bolted joints are prevalent in most assembled structures; however, predictive models for their behavior do not exist. Calibrated models, such as the Iwan model, are able to predict the response of a jointed structure over a range of excitations once calibrated at a nominal load. The Iwan model, though, is not widely adopted due to the high computational expense of implementation. To address this, an analytical solution of the Iwan model is derived under the hypothesis that for an arbitrary load reversal, there is a new distribution of dry friction elements, which are now stuck, that approximately resemble a scaled version of the original distribution of dry friction elements. The dry friction elements internal to the Iwan model do not have a uniform set of parameters and are described by a distribution of parameters, i.e. which internal dry friction elements are stuck or slipping at a given load, that ultimately governs the behavior of the joint as it transitions from microslip to macroslip. This hypothesis allows the model to require no information from previous loading cycles. Additionally, the model is extended to include the pinning behavior inherent in a bolted joint. Modifications of the resulting framework are discussed to highlight how the constitutive model for friction can be changed (in the case of an Iwan-Stribeck formulation) or how the distribution of dry friction elements can be changed

Sandia National Laboratories[1], Albuquerque, NM, USA

William Marsh Rice University, Houston, TX, USA

[1]: *Sandia National Laboratories is a multi-mission laboratory managed and operated by Sandia Corporation, a wholly owned subsidiary of Lockheed Martin Corporations, for the U.S. Department of Energy's National Nuclear Security Administration under Contract DE-AC04-94AL85000.*

E-mail: brake@rice.edu

(as is the case for the Iwan plasticity model). The Reduced Iwan Plus Pinning (RIPP) model is then applied to the Brake-Reuß beam in order to discuss methods to deduce model parameters from experimental data.

Keywords Joint Mechanics · Iwan Model · Pinning · Friction

1 Introduction

One of the great remaining challenges in classical structural dynamics and solid mechanics is the prediction of the behavior of a jointed connection. Despite the prevalence of jointed connections in engineering structures, predictive models do not exist for several reasons: in most applications there is no penalty for over designing a joint to ensure that it survives most realistic loading scenarios, the physics to predict the behavior of a joint is reliant upon an improved understanding of friction (which is a nontrivial undertaking), and the joint models that do exist are often computationally burdensome (which results in analysts favoring simplistic and hopefully conservative representations instead). However, in several industries (aerospace, defense, automotive, etc.) there is becoming a pressing need to better understand the behavior of a jointed connection. In many of the pertinent applications, the jointed connections are part of a system that will only be fabricated a small number of times and that has strict weight and space limits (increasing the penalty for over designing the joint). Conventional approaches to modeling the joint, due to harsh loading environments and nonlinearities, often are not as conservative as an analyst anticipates. In fact, the use of linear models, calibrated at high excitation levels, significantly under predict the energy dissipation and joint stiffness at low load levels. Consequently, a number of failures have been reported in recent years that are related to bolted joints (see, for instance, (Deckstein and Traufetter 2012)).

The present research is motivated by one particular class of joint models that are used in finite element analysis as well as analytical mechanics and reduced order models: the Iwan model. The broad category of constitutive models referred to as Iwan models are used to model dissipative behavior with a single element. These models originally were applied to elastic-plastic material responses (Iwan 1966; Iwan 1967) and have more recently been adapted to joint mechanics (Segalman 2005; Segalman and Starr 2004). In particular, the four-parameter Iwan model (Segalman 2005) reg-

ularizes the joint interface to be represented by a single element, which contains many internal degrees of freedom. The four-parameter Iwan model is, essentially, a constitutive model that describes the hysteretic behavior of micro- and macroslip across a jointed interface and replaces the kinematics of the adjacent interfacial surfaces with a nonlinear constitutive model. The model's constitutive parameters can be populated either with representative experimental data or deduced from fine mesh finite element analysis. The constitutive formulation is fundamentally that of a Preisach model and has basis in (Bauschinger 1886; Masing 1926; Prandtl 1928; Ishlinskii 1944; Iwan 1966; Iwan 1967). More recently, the Iwan model has been extended to be considered in modal space (as opposed to physical coordinates) (Deaner et al. 2013).

One difficulty present in the implementation of the Iwan model is its high computational cost. The common set of Iwan models used for the analysis of bolted joints are based on a discretized set of dry friction sliders (Segalman 2005). This discretization leads to the need to store the individual state of each dry friction slider in the model, effectively increasing the degrees of freedom from one to an arbitrarily large number (each of which corresponds to a nonlinear, discontinuous system, which can lead to significant numerical challenges (Van de Vrande, Van Campen, and de Kraker 1999)). In what follows, a reduced formulation of the Iwan model is derived based on the assumption that when a load reversal occurs, the collective state of the dry friction sliders resembles a scaled version of the original distribution of dry friction sliders (this assumption is discussed in Section 2.3.1). While this is a subtle change from the four-parameter Iwan model formulated in (Segalman 2005), both the new and old models are still approximations that can be calibrated to fit the data accurately, and the resulting model thus does not lose applicability from this new assumption.

2 Analytical Development

Conceptually, there are three distinct regimes for the model, as can be seen in Fig. 1: microslip ($0 \leq \varphi < \phi_{MAX}$), macroslip ($\phi_{MAX} \leq \varphi < \delta_P$), and pinning ($\delta_P \leq \varphi$). In what follows, the force in these three regimes is calculated as part of two separate calculations: one calculation for the force due to the Iwan model, which includes micro- and macroslip, and one calculation for the pinning force. This division is necessitated as the Iwan model is based on the relative displacement across the joint

u while the pinning forces are based on the global displacement of the joint φ.[1]

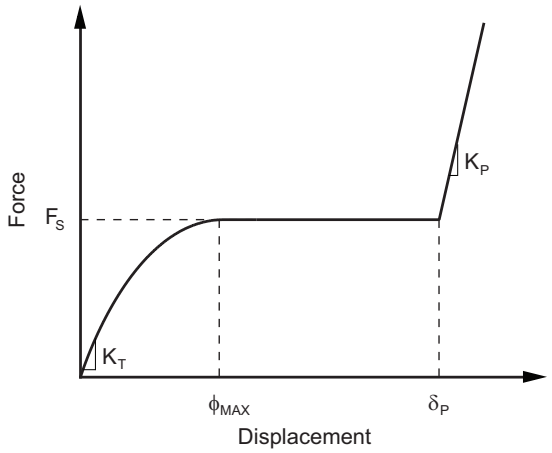

Fig. 1 Illustrative drawing of the constitutive force F for a bolted joint as a function of displacement φ.

2.1 Pinning Force

The pinning force occurs when the shank of the bolt engages the edge of the through hole (of diameter $2\delta_P$) in which it is located. This contact is thus between two cylindrical surfaces. If no plasticity is assumed to occur, this can be modeled using Hertz's (Johnson 1985) elastic contact formulation for two cylinders[2]

$$F_{PIN} = \frac{\pi}{4} E^* L d. \tag{1}$$

For this formulation, E^* is the effective modulus of the two materials in contact (each having elastic modulus E_j and Poisson's ratio ν_j)

$$E^* = \left(\frac{1-\nu_1^2}{E_1} + \frac{1-\nu_2^2}{E_2} \right)^{-1}. \tag{2}$$

The engagement length of the bolt's shank with the through hole (i.e. the height of the hole) is L, and $d = \varphi - \delta_P$ is the interference/contact displacement of the two surfaces. As (1) is linear in d, F_{PIN} can be expressed as a spring force $F_{PIN} = K_P d$ with stiffness

$$K_P = \frac{\pi}{4} E^* L. \tag{3}$$

Thus, all parameters needed to define K_P are based on material and geometric properties, which can be easily determined.

2.2 Relation of Relative and Global Displacements for the Iwan and Pinning Forces

In what follows, the relative displacement u is defined to be positive in the slip direction. Additionally, δ_0 is defined to be the global displacement of the system at the start of a slip event (e.g. a load reversal), and F_0 is defined to be the force due to the Iwan element at the start of a slip event (i.e. from the previous loading cycle). In order to

[1] Thus, the three regimes defined above hold for a narrow range of u and φ, including when $u = \varphi$. Otherwise, microslip and macroslip must be defined in terms of u and pinning must be defined in terms of φ.

[2] Technically, Hertz's formulation is for two cylinders contacting each other, not one cylinder inside another cylinder. However, it is assumed that this case can be represented with Hertz's model without loss of accuracy.

relate the force due to the Iwan model and the force due to pinning,

$$\varphi = \delta_0 \pm u \tag{4}$$

($+u$ for forward motion, $-u$ for backward motion due to u being positive in the slip direction). This relationship establishes the constraint that for $\delta_0 \pm u \mp \delta_P \geq 0$, the pinning force is engaged

$$F_{PIN} = \pm H(\delta_0 \pm u \mp \delta_P) \times K_P(\delta_0 \pm u \mp \delta_P), \tag{5}$$

with the Heaviside step function $H(\cdot)$ used to specify pinning forces only when the bolt shank engages the bolt hole.

2.3 Four-Parameter Iwan Model Overview

To model the forces in both the micro- and macroslip regimes, the Iwan model is proposed. As a starting point, the four parameter Iwan model developed in (Segalman 2005) is used. In that research, the constitutive representation for the Iwan model is

$$F_{IWAN} = \int_0^\infty \rho(\phi)\,(u(t) - x(t,\phi))\,\mathrm{d}\phi, \tag{6}$$

which describes a distribution $\rho(\phi)$ of dry friction sliders (i.e. Jenkins elements, originally attributed to (Jenkins 1962)) such as shown in Fig. 2. The distribution, $\rho(\phi)$, represents the number of sliders that slip when stretched a distance ϕ. The units of ρ are force/length^2, which comes from the original formulation of (Segalman 2005) convoluting the distribution ρ with the stiffness common to all of the dry friction sliders (K in Fig. 2). As is seen later with the discussion beginning around Eq. 12, the displacement ϕ across each slider is the amount that a slider is stretched (i.e. ϕ is not a relative displacement of the joint, but rather a relative stretching of each dry friction slider). Thus, at some displacement ϕ, $\rho(\phi)/c$ sliders begin to slip (here, c is a normalization constant to account for the units of ρ). Note that in (Segalman 2005), the global displacement U is used in place of the relative displacement u; this substitution is made, though, without loss of generality in what follows due to the introduction of F_0 and δ_0, mentioned above. The j^{th} slider has instantaneous displacement $x_j = x(t, \phi_j)$, and transitions from sticking to sliding at a displacement of $x_j = \phi_j$. The choice of distribution $\rho(\phi)$ is a nontrivial task, and several choices are discussed in what follows. For the model proposed in (Segalman 2005), the general form of the resulting hysteresis loop is illustratively shown in Fig. 3.

The four-parameter Iwan model of (Segalman 2005) is subject to the two Masing conditions (which are both visible in Fig. 3): 1) the forward and back-

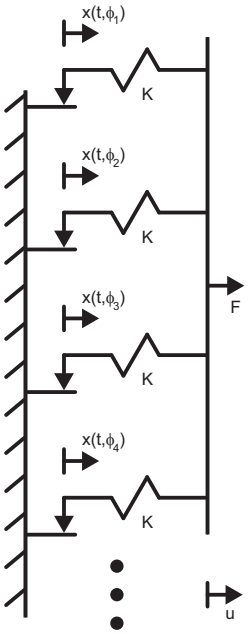

Fig. 2 Illustrative drawing of an Iwan model as a parallel arrangement of dry friction sliders.

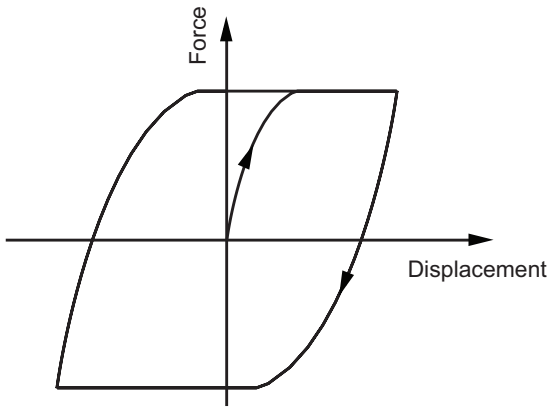

Fig. 3 Illustrative drawing of a typical hysteresis curve for a four-parameter Iwan model described by (Segalman 2005).

ward curves are reflections of one another and are scaled to fit between the initiation of the loading point and the force for macroslip, and 2) that if a trajectory intersects the curve of a previous loading cycle, then it will change to follow the previous curve. In what follows, the first Masing condition is exploited: a displacement in the negative direction is the same as a displacement in the positive direction with a change of coordinates. The second Masing condition, though, due to possible transitions from microslip to macroslip to pinning, is not applied in vibratory environments. In a quasi-static framework, in which the model oscillates between two extreme forces, the second Masing condition will still hold; but in vibratory environments, the applicability of the second Masing condition is less clear, and is neglected (see, for instance, the results of Section 3). By assuming that this condition can be neglected, the need for a record of the history of previous loading cycles is eliminated from this reduced formulation (thus removing a challenge that is evident in models such as (Smallwood, Gregory, and Coleman 2001; Segalman and Starr 2004)).

The distinguishing feature of the four parameter Iwan model is the proposed distribution of Jenkins elements $\rho(\phi)$, which specifies the number of dry friction sliders internal to the Iwan element that slip after being stretched a distance ϕ. In (Segalman 2005), the proposed distribution

(shown in Fig. 4(a)) is

$$\rho(\phi) = R\phi^{\chi}\left(H(\phi) - H(\phi - \phi_{MAX})\right) + S\delta(\phi - \phi_{MAX}) \quad (7)$$

$$R = \frac{F_S(\chi+1)}{\phi_{MAX}^{\chi+2}\left(\beta + \frac{\chi+1}{\chi+2}\right)} \quad (8)$$

$$S = \frac{F_S}{\phi_{MAX}}\left(\frac{\beta}{\beta + \frac{\chi+1}{\chi+2}}\right) \quad (9)$$

$$\phi_{MAX} = \frac{F_S(1+\beta)}{K_T\left(\beta + \frac{\chi+1}{\chi+2}\right)}, \quad (10)$$

with Delta function $\delta(\cdot)$. In this formulation, $3+\chi$ is the energy dissipated per cycle of small amplitude oscillation ($-1 < \chi \leq 0$ is therefore permissible in this model). The distribution ρ is a power law relationship that is truncated at ϕ_{MAX} by a Delta function. The ratio of the stiffness of the Delta function portion of the distribution S to the power law portion of the distribution R is defined as β

$$\beta = \frac{S}{R\phi_{MAX}^{\chi+1}/(\chi+1)}, \quad (11)$$

and is typically determined from measurements of dissipation versus excitation amplitude (Deaner et al. 2015). Note that with the definition of β, the model of (Segalman 2005) can be posed in terms of F_S, K_T, χ, and β, as opposed to a different set of parameters that are more difficult to measure directly (e.g. F_S, R, S, and ϕ_{MAX}).[3] The relationships of Eqs. 8-10 are developed in (Segalman 2005) with this ease of model parameter determination in mind.

[3] Though, the measurement of ϕ_{MAX} instead of F_S is often more practical as testing to macroslip is not always feasible.

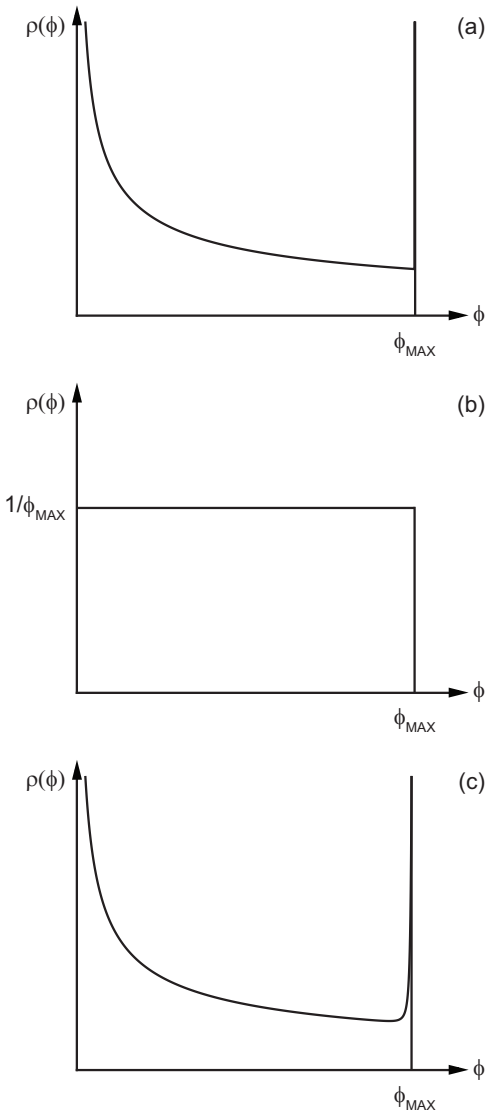

Fig. 4 Illustrations of (a) the distribution of (Segalman 2005), (b) the uniform distribution of (Iwan 1966), and (c) Segalman's proposed distribution.

With the definition of u in Eq. 4 the quantity from Eq. 6

$$u - x(t,\phi) = \begin{cases} u & \text{if slider } \phi \text{ is stuck} \\ \phi & \text{if slider } \phi \text{ is sliding.} \end{cases} \quad (12)$$

The slip function Γ can then be defined as

$$\Gamma(u,\phi) = u - x(t,\phi) = \begin{cases} u & u < \phi \\ \phi & u \geq \phi. \end{cases} \quad (13)$$

Substituting Γ and ρ into Eq. 6 yields

$$F_{IWAN} = \int_0^{\phi_{MAX}} \Gamma(u,\phi) R \phi^{\chi} \mathrm{d}\phi + S\Gamma(u,\phi_{MAX}). \quad (14)$$

Based on Γ, this can be broken into two integrals

$$F_{IWAN} = \int_0^{u} R\phi^{\chi+1}\mathrm{d}\phi + \int_u^{\phi_{MAX}} uR\phi^{\chi}\mathrm{d}\phi + S\Gamma(u,\phi_{MAX}), \quad (15)$$

which has solution

$$F_{IWAN} = R\left(\left(\frac{1}{\chi+2} - \frac{1}{\chi+1}\right)u^{\chi+2} + \frac{\phi_{MAX}^{\chi+1}}{\chi+1}u\right) + S\Gamma(u,\phi_{MAX}). \quad (16)$$

Substituting Eqs. 8 and 9 gives the full expression for the Iwan forces

$$F_{IWAN} = \frac{F_S(\chi+1)}{\phi_{MAX}^{\chi+2}\left(\beta + \frac{\chi+1}{\chi+2}\right)} \times \left(\left(\frac{1}{\chi+2} - \frac{1}{\chi+1}\right)u^{\chi+2} + \frac{\phi_{MAX}^{\chi+1}}{\chi+1}u\right) + \frac{F_S}{\phi_{MAX}}\frac{\beta}{\beta + \frac{\chi+1}{\chi+2}}\Gamma(u,\phi_{MAX}). \quad (17)$$

In the limiting case of $u \geq \phi_{MAX}$, the Iwan force reduces to $F_{IWAN} = F_S$.

2.3.1 Considerations for Cyclic Loading

Two cases must be considered for the cyclic loading: loading to macroslip, and loading within the microslip regime. In loading to macroslip, all of the Jenkins sliders are, by definition, in slip, and the first Masing condition can be applied. For the first cycle of loading, it is assumed that $F_0 = 0$ and $\delta_0 = 0$. After the first cycle in which the joint is in macroslip, $F_0 = F_S$ (as F_0 doesn't include pinning forces), and each Jenkins element is fully stretched in the direction opposite from the new loading direction. For oscillations between two extremes (i.e. $-F_S$ and F_S), the first Masing condition (Segalman 2005; Jayakumar 1987) yields

$$F_+(u) = -F_S + 2F_{IWAN}\left(\frac{\varphi - \delta_0}{2}\right) \quad (18)$$

$$F_-(u) = -F_S - 2F_{IWAN}\left(\frac{\delta_0 - \varphi}{2}\right). \quad (19)$$

The forces F_+ and F_- are for positive and negative loading cycles respectively, which result in Eqs. 18 and 19 having the form

$$F_\pm = \mp F_S \pm \gamma F_{IWAN}\left(\frac{\pm\varphi \mp \delta_0}{\gamma}\right), \quad (20)$$

where γ scales the function appropriately.

In many vibratory environments, however, the limits of oscillation are not necessarily between the two extreme values. Therefore, an incomplete

case (e.g. never loading to the point of macroslip) must be considered. In the previously defined relative coordinate system for u, after a load reversal, $-F_0 > -F_S$, the Jenkins elements of strength ϕ are fully stretched in the direction opposite from the new loading direction for $\phi < u_0$, and are stretched a distance u_0 in the direction opposite from the new loading direction for $\phi > u_0$. As a result, Eq. 15 becomes

$$F_{IWAN} = \int_0^u R\left(\frac{\phi}{2}\right)^{\chi+1} \mathrm{d}\phi + \int_u^{\phi_{MAX}} uR\phi^{\chi}\mathrm{d}\phi + S\Gamma(u,\phi_{MAX}) - F_0, \quad (21)$$

for $u \leq 2u_0$, and, with $\psi = \phi - 2u_0$,

$$F_{IWAN} = \frac{1}{2^{\chi+1}}\int_0^{2u_0} R\phi^{\chi+1}\mathrm{d}\phi + \int_{2u_0}^{u} R\psi^{\chi+1}\mathrm{d}\psi + \int_u^{\phi_{MAX}} uR\phi^{\chi}\mathrm{d}\phi + S\Gamma(u,\phi_{MAX}) - F_0 \quad (22)$$

for $u > 2u_0$. The form of Eq. 22 is a (nonlinearly) scaled version of Eq. 15. Thus, the hypothesis is proposed:

Hypothesis For an arbitrary load reversal, there is a new distribution of Jenkins elements, which are now stuck, that approximately resemble a scaled version of the original distribution of Jenkins elements.

As a first order approximation of the new distribution, a linear scaling function is used in which γ is bounded by $0 < \gamma \leq 2$. This leads to the functional form

$$F_{SLIDING} = \begin{cases} F_0 + \frac{F_S - F_0}{F_S} F_{IWAN}\left(u\frac{F_S}{F_S - F_0}\right) & \text{loading} \\ F_0 - \frac{-F_S - F_0}{-F_S} F_{IWAN}\left(-u\frac{-F_S}{-F_S - F_0}\right) & \text{reverse loading} \end{cases} \quad (23)$$

This is rewritten as

$$F_{SLIDING} = F_0 + \frac{F_S \mp F_0}{F_S} F_{IWAN}\left(\pm u\frac{F_S}{F_S \mp F_0}\right), \quad (24)$$

using the F_{IWAN} defined in Eq. 17. This relationship is predicate on F_0 being a global value such that $-F_S \leq F_0 \leq F_S$. The complete formulation for the RIPP joint model can now be expressed as

$$F_{RIPP} = F_{PIN} + F_{SLIDING}. \quad (25)$$

In the case of $\delta_0 \geq \delta_P - \phi_{MAX}$, this implies that macroslip is not necessary to achieve pinning. It should be noted, however, that the force F_0 should be determined solely from $F_{SLIDING}$ in order for the model to be consistent.

2.3.2 Comparison With the Discrete Four-Parameter Iwan Model

As a verification of the analytical RIPP joint formulation, Fig. 5 compares the RIPP joint model (25) to the discretized four-parameter Iwan model of (Segalman 2005) on which it is based. The parameters for (Segalman 2005) are chosen based on a 304 Stainless Steel lap joint, such as found in (Segalman et al. 2009), and are listed in Table 1. The range for the displacement to calculate the hysteresis curve is specified as ±2.25 mm. Outside of the pinning region, the two curves are coincident. Near the transition from microslip to macroslip, the discretization of (Segalman 2005) is evident under high magnification (as the curve appears faceted), but at the scale shown the two models are in complete agreement.

Property	Value
Tangential Stiffness, K_T	1.5×10^7 N/m
Macroslip Force, F_S	4 kN
Dissipation Exponent, χ	-0.5
Stiffness Ratio, β	0.005
Pinning Stiffness, K_P	10^7 N/m
Pinning Clearance, δ_P	2 mm

Table 1 Joint parameters.

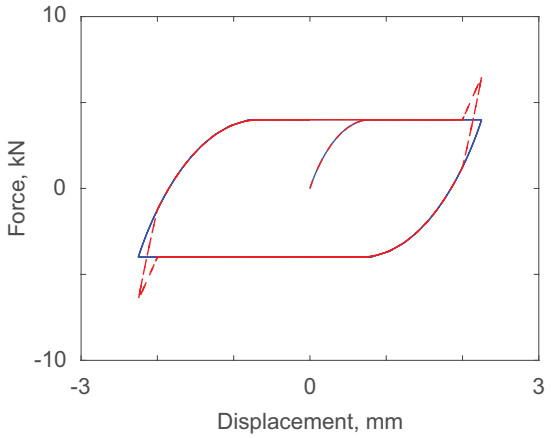

Fig. 5 Hysteresis curves for the discretized four-paramter Iwan model of (Segalman 2005) (—), and the RIPP joint model (– –).

2.4 Extension to the Five-Parameter Iwan Model

The five-parameter Iwan model, proposed by Mignolet (Wang and Mignolet 2014), belongs to a class of split Iwan models in which the response is split into two regimes. The fifth parameter is defined as the ratio between dynamic μ_D and static μ_S friction

$$\theta = \frac{\mu_D}{\mu_S}. \tag{26}$$

The conceptual split in this model is that once a Jenkins element begins to slide, it is governed by dynamic friction rather than the static friction that governed it in the stick state. The proposed distribution $\rho(\phi)$, though, remains the same. Con-

sequently, the Iwan force becomes

$$F_{IWAN} = \theta \int_0^u R\phi^{\chi+1} \mathrm{d}\phi + \int_u^{\phi_{MAX}} uR\phi^{\chi} \mathrm{d}\phi + S\Gamma(u, \phi_{MAX}). \quad (27)$$

In the limiting case of $\theta = 1$, this reduces to Eq. 15. As before, the solution follows that

$$F_{IWAN} = R\left(\left(\frac{\theta}{\chi+2} - \frac{1}{\chi+1}\right) u^{\chi+2} + \frac{\phi_{MAX}^{\chi+1}}{\chi+1} u\right) + S\Gamma(u, \phi_{MAX}). \quad (28)$$

Substituting R and S yields the final form of the Iwan force equation for the five-parameter Iwan model

$$F_{IWAN} = \frac{F_S(\chi+1)}{\phi_{MAX}^{\chi+2}\left(\beta + \frac{\chi+1}{\chi+2}\right)} \times \left(\left(\frac{\theta}{\chi+2} - \frac{1}{\chi+1}\right) u^{\chi+2} + \frac{\phi_{MAX}^{\chi+1}}{\chi+1} u\right) + \frac{F_S}{\phi_{MAX}} \frac{\beta}{\beta + \frac{\chi+1}{\chi+2}} \Gamma(u, \phi_{MAX}). \quad (29)$$

In the limiting case of $u \geq \phi_{MAX}$,

$$F_{IWAN} = F_S \frac{\beta + \theta\frac{\chi+1}{\chi+2}}{\beta + \frac{\chi+1}{\chi+2}}, \quad (30)$$

which is less than F_S for $\theta < 1$.

In Fig. 6, the RIPP joint model of the four-parameter Iwan model is compared to the RIPP joint model of the five-parameter Iwan model with $\theta = 0.75$ and all other parameters the same as before. Both models exhibit the same tangent stiffness immediately after a load reversal; however the five-parameter model has a lower peak force due to $\theta < 1$. One unexpected consequence of this (coupled with the neglecting of the second Masing condition, as mentioned above) is that the maximum and minimum forces vary from one loading cycle to the next.

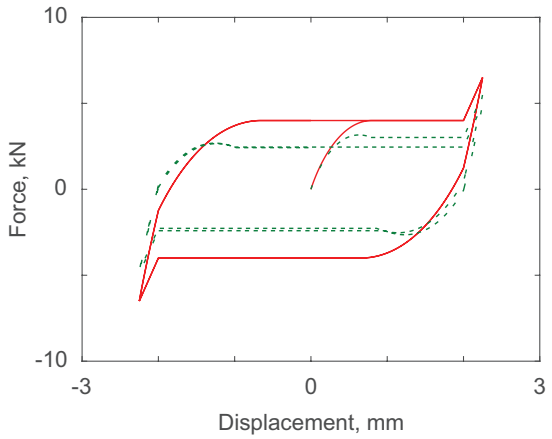

Fig. 6 Hysteresis curves for the RIPP joint model of the four-parameter Iwan model (—), and of the five-parameter Iwan model with $\theta = 0.75$ (– –).

2.5 Extension to the Uniform Iwan Distribution

In (Iwan 1966), the Iwan element is formulated with a uniform distribution for ρ (Fig. 4(b)) in order to represent energy dissipation due to plastic processes. The width of the distribution for the present work is taken to be ϕ_{MAX}, with a height of $1/\phi_{MAX}$. This distribution leads to the Iwan force

$$F_{IWAN} = \int_0^{\phi_{MAX}} \frac{c}{\phi_{MAX}} \Gamma(u, \phi) \mathrm{d}\phi. \quad (31)$$

The constant c is determined by setting the resulting solution equal to F_S, yielding

$$F_{IWAN} = \begin{cases} \frac{2F_S}{\phi_{MAX}} \left(u - \frac{u^2}{2\phi_{MAX}} \right) & u < \phi_{MAX} \\ F_S & u \geq \phi_{MAX}. \end{cases} \tag{32}$$

Using the same parameters as from Fig. 5, Fig. 7 compares the hysteresis curves for the RIPP joint model of the four-parameter Iwan model to that of the uniform distribution Iwan model. Due to the uniform distribution for $\rho(\phi)$, the tangent stiffness appears much lower than for the four-parameter Iwan model. By definition, the macroslip forces and pinning behavior is the same for the two models though.

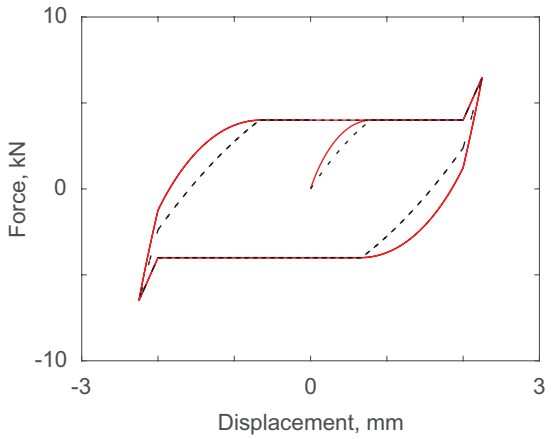

Fig. 7 Hysteresis curves for the RIPP joint model of the four-parameter Iwan model (—), and of the uniform distribution Iwan model (– –).

2.6 Extension to Other Distribution Functions

The three models discussed above form a subset of all possible Iwan-type models. The distribution proposed in (Segalman 2005) is an approximation itself as a more accurate model requires both more parameters and more experimental data than is available (e.g. data on the break-free force for a joint). A plausible model, though, is suggested by Dan Segalman to resemble the curve shown in Fig. 4(c). A potential mathematical form for this model is

$$\rho(\phi) = R\phi^{\chi} + S\left(\phi_{MAX} - \phi\right)^{-\gamma}. \tag{33}$$

In this model, $\gamma > 0$ and S is not necessarily the same as proposed in (Segalman 2005) due to scaling issues. This precise form, of course, has no solution for $\phi = \phi_{MAX}$, which could easily be resolved by truncating $\rho(\phi)$ for $\phi_{MAX} - \epsilon \leq \phi \leq \phi_{MAX}$ (where $\epsilon \ll \phi_{MAX}$); however, without experimental data to better quantify the nature of this distribution, any solution would be ad hoc and speculative.

2.7 Extension to Higher Order Friction Models

Another potential Iwan model is the Iwan-Stribeck[4] model (for discussions of the Stribeck friction model,

[4] This model is proposed purely as an example of how to apply the RIPP joint formulation to other constitutive models. The burden associated with parameter es-

see (Armstrong-Hélouvry, Dupont, and Canudas de Wit 1994; Gaul and Nitsche 2000; Gaul and Nitsche 2001)). This model is proposed as a method to smooth out the nonlinearity introduced by the split five-parameter Iwan model of (Wang and Mignolet 2014). The Stribeck friction model postulates that the friction force is

$$F(v) = \left(F_C + (F_S - F_C) e^{-\left(\frac{v}{v_S}\right)^{\delta_S}} \right) \text{sign}(v) + F_V v, \tag{34}$$

which introduces the parameters F_C as the friction force level that is proportional to the normal load, F_S as the stiction force (which is equal to the previously defined macroslip force F_S), F_V as a viscous damping term due to lubrication viscosity, and empirically defined quantities v_S and δ_S. Previous studies of the Stribeck friction model typically define $\delta_S \in [1/2, 2]$, with $\delta_S = 2$ corresponding to the Gaussian model (Armstrong-Hélouvry, Dupont, and Canudas de Wit 1994). For very large values of δ_S, this corresponds to a system with an effective boundary lubricant. From the five-parameter Iwan model, F_C and F_S are related via

$$\theta = \frac{F_C}{F_S}. \tag{35}$$

timation is too high to consider this a practical model for analysts to use.

Using the distribution $\rho(\phi)$ defined in (Segalman 2005), this results in an eight-parameter Iwan model.[5] Despite the burden placed on the analyst to populate the parameters of these models, the derivation of a RIPP joint representation is straightforward. For an imposed state with system slip displacement u and sliding velocity v, the total force acting through the joint system for a discrete number of friction sliders is

$$F = \sum_{\tilde{\phi}_i \geq ku} ku + \sum_{\tilde{\phi}_i \leq ku} \theta \tilde{\phi}_i + \left(F_S(1-\theta) e^{-\left(\frac{v}{v_S}\right)^{\delta_S}} \right) \text{sign}(v) + F_V v. \tag{36}$$

In the original nomenclature of (Iwan 1966; Segalman and Starr 2004), $\tilde{\phi}_i$ is the slip force for the i^{th} slider, k is the stiffness common to all of the friction sliders, and the population density function is expressed as $\tilde{\rho}(\tilde{\phi}_i)$. Following the derivation of (Segalman and Starr 2004), the summation of forces over an infinite number of sliders yields the

[5] For an even more burdensome model, consider the seven-parameter friction model in (Armstrong-Hélouvry, Dupont, and Canudas de Wit 1994), with the $\rho(\phi)$ from (Segalman 2005); this results in a ten-parameter Iwan model!

integral form of the force equation

$$F = ku\int_{ku}^{\infty}\tilde{\rho}(\tilde{\phi})\mathrm{d}\tilde{\phi} + \int_{0}^{ku}\tilde{\rho}(\tilde{\phi})\left(\theta\tilde{\phi} + \left(F_S(1-\theta)e^{-\left(\frac{v}{v_S}\right)^{\delta_S}}\right)\mathrm{sign}(v) + F_V v\right)\mathrm{d}\tilde{\phi}. \quad (37)$$

Using a change of variables ($\phi = \tilde{\phi}/k$ and $\rho(\phi) = k^2\tilde{\rho}(k\phi)$) yields

$$F = u\int_{u}^{\infty}\rho(\phi)\mathrm{d}\phi + \frac{1}{k}\left(F_S(1-\theta)e^{-\left(\frac{v}{v_S}\right)^{\delta_S}}\mathrm{sign}(v) + F_V v\right)\int_{0}^{u}\rho(\phi)\mathrm{d}\phi + \theta\int_{0}^{u}\phi\rho(\phi)\mathrm{d}\phi. \quad (38)$$

The common spring stiffness k is related to known parameters via $k\phi_{MAX} = F_S$. Using the same $\rho(\phi)$ as in (Segalman 2005), the (eight-parameter) Iwan-Stribeck model's force becomes

$$F_{IWAN} = \frac{F_S(\chi+1)}{\phi_{MAX}^{\chi+2}\left(\beta+\frac{\chi+1}{\chi+2}\right)} \times \left(\left(\frac{\theta}{\chi+2}-\frac{1}{\chi+1}\right)u^{\chi+2} + \frac{\phi_{MAX}^{\chi+1}}{\chi+1}u\right) + \frac{F_S}{\phi_{MAX}}\frac{\beta}{\beta+\frac{\chi+1}{\chi+2}}\Gamma(u,\phi_{MAX}) + \frac{1}{\beta+\frac{\chi+1}{\chi+2}}\left(F_S(1-\theta)e^{-\left(\frac{v}{v_S}\right)^{\delta_S}}\mathrm{sign}(v) + F_V v\right) \times \frac{u^{\chi+1}}{\phi_{MAX}^{\chi+1}}. \quad (39)$$

Note that the sign(v) term can be neglected by using the relative definition of u in which displacements and, consequently, velocities, always occur in a positive reference frame. In the extreme case of $v_S = F_V = 0$, the five-parameter model is recovered (as the sign(0) = 0 property is important in this extreme case).

The hysteresis curve for the Iwan-Stribeck model, with $\theta = 0.75$, $F_V = 1$ mN·s/m, $v_S = 0.1$ mm/s, and $\delta_S = 2$ is shown in Fig. 8 for three different loading rates. At the highest loading rate (4 mm/s), the initial loading portion of the hysteresis curve is identical to the five-parameter Iwan model (shown in Fig. 6) up until the first load reversal, at which point the Iwan-Stribeck model predicts a more compliant response. At lower loading rates, the Iwan-Stribeck model appears significantly more stiff than the four-parameter Iwan model. It is worth noting, though, that in dynamic applications, the loading rate is not a constant value as used here.

The extension of the RIPP joint formulation to other, phenomenologically different friction models is easily managed following a similar procedure as for the Iwan-Stribeck model. For multi-dimensional models that couple in-plane and out-of-plane forces, such as (Petrov and Ewins 2004; Cigeroglu, An, and Menq 2007), the present framework is not compatible for this type of coupling, and this is an area of active research.

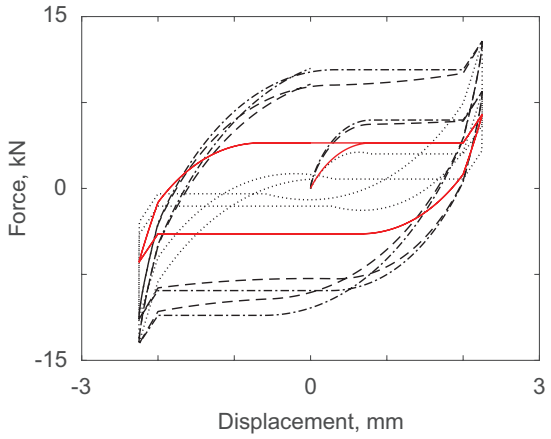

Fig. 8 Hysteresis curves for the RIPP joint model of the four-parameter Iwan model (—), and of Iwan-Stribeck model for loading rates of 0.4 μm/s (– · –), 40 μm/s (– –), and 4 mm/s(· · ·).

3 Dynamic Response of the RIPP Joint Models

The significant difference between the Iwan model and the Iwan-Stribeck model is attributable to the quasi-static nature of the hysteresis curve calculation (i.e. the constant velocity). To assess these models dynamically, a single degree of freedom system with mass 1 kg is connected to ground through a joint element (both the discretized four-parameter Iwan model and the RIPP joint models discussed are used). The mass is excited by an applied force of $5\sin(100\times 2\pi t)$ kN, and the joint parameters are the same as in Table 1. The first 50 ms of the transient response is shown in Figs. 9 and 10 for the five different models (the discretized 4-parameter Iwan model of (Segalman 2005), the 4-parameter Iwan model RIPP joint formulation, the 5-parameter Iwan model RIPP joint formulation, the uniform distribution RIPP joint formulation, and the Iwan-Stribeck RIPP joint model). The effect of pinning is clearly discernible from the responses of the 4-parameter RIPP joint model and the 4-parameter discretized Iwan model in Fig. 9. If pinning is not considered, the results from the discretized 4-parameter Iwan model and the 4-parameter Iwan model RIPP joint formulation are identical, which is paramount as small differences in the constitutive model for nonlinearities within a system can lead to very large differences in optimal design of the system (Brake 2014). In Fig. 10, the 5-parameter RIPP joint model and the Iwan-Stribeck RIPP joint models are nearly coincident for the viscous parameters used (which are representative of dry contact). This is an encouraging result as it shows that two phenomenologically different friction models are converging towards predicting the same behavior in this system.

The hysteresis plots from the transient dynamic simulations are shown in Figs. 11 and 12. Due to the vibratory environment, multiple loading and unloading cycles are observed near the extremities of the displacement values. In particular, each

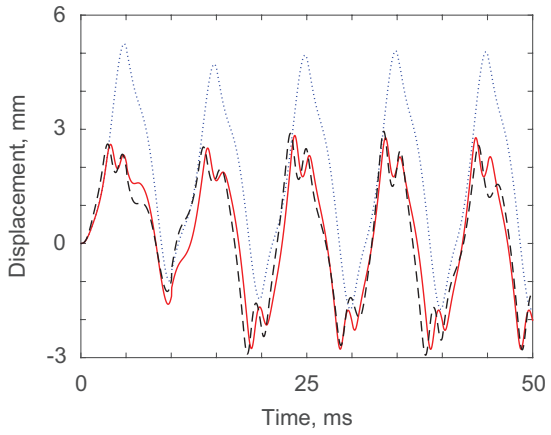

Fig. 9 Transient response of the single degree of freedom oscillator attached to a discretized four-parameter Iwan model from (Segalman 2005) (· · ·), the RIPP joint representation of the four-parameter Iwan model (—), and an a uniform distribution RIPP joint model (– –).

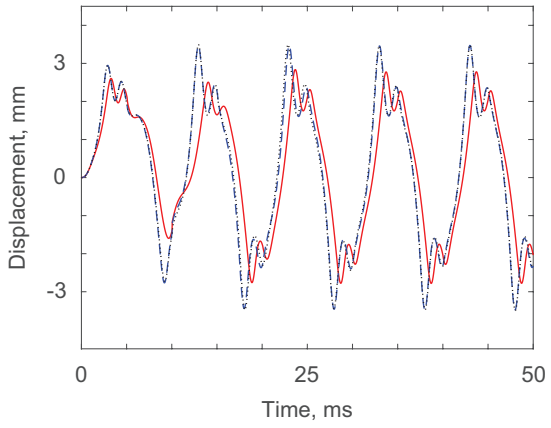

Fig. 10 Transient response of the single degree of freedom oscillator attached to the RIPP joint representation of the four-parameter Iwan model (—), the RIPP joint model for the five-parameter Iwan model with $\theta = 0.75$ (– –), and the Iwan-Stribeck RIPP joint model (· · ·).

of the RIPP joint models shows behavior in which pinning occurs, the slip direction reverses but does not achieve macroslip in the opposite direction before reversing again and initiating pinning once more. After several impacts between the bolt shank and bolt hole, the applied force is sufficient to initiate macroslip in the opposite direction before this process is repeated again. By contrast, the discretized four-parameter Iwan model, which does not include pinning, exhibits no such rebound dynamics. This is to be expected as pinning creates a non-smooth nonlinearity in the macroslip regime. Similar to the results in Fig. 10, the five-parameter RIPP joint model and the Iwan-Stribeck RIPP joint model are coincident in Fig. 12, in contrast to Fig. 8 (in which the loading rate was constant).

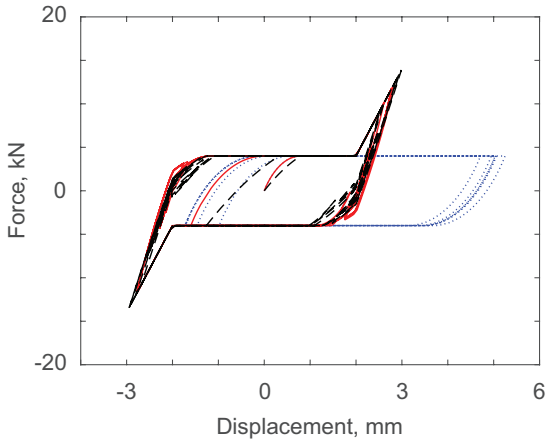

Fig. 11 Dynamic hysteresis plot of the single degree of freedom oscillator attached to a discretized four-parameter Iwan model from (Segalman 2005) (· · ·), the RIPP joint representation of the four-parameter Iwan model (—), and an a uniform distribution RIPP joint model (– –).

For each of the analytical Iwan models, a significant reduction in computation time compared

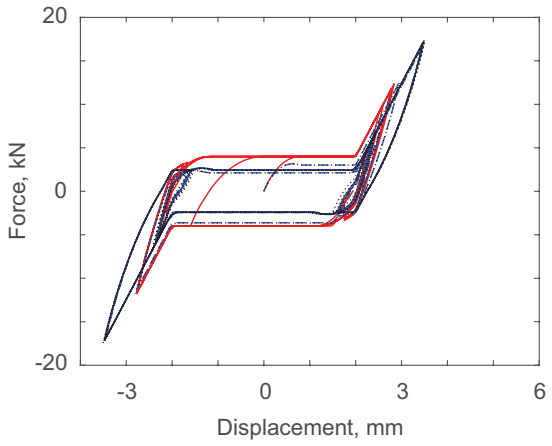

Fig. 12 Dynamic hysteresis plot of the single degree of freedom oscillator attached to the RIPP joint representation of the four-parameter Iwan model (—), the RIPP joint model for the five-parameter Iwan model with $\theta = 0.75$ (– –), and the Iwan-Stribeck RIPP joint model ($\cdots$).

to the discretized four-parameter Iwan model is observed. To calculate the quasi-static hysteresis loops or the dynamic response, the computational time of the discretized four-parameter Iwan model is observed to be a factor of three longer than the analytical formulation (both when pinning is and is not active). For comparing the other analytical model to the discretized model, the Mignolet distribution is also approximately a factor of three faster, the uniform distribution is an order of magnitude faster, and the Iwan-Stribeck model is a factor of two faster for the quasi-static hysteresis loops and approximately 25% faster for the dynamic simulations. To quantify the performance of the analytical models more accurately, a more realistic simulation should be used that is representative of a real assembly; the numbers provided here are for illustrative purposes.

4 Parameter Estimation

This section is provided as an example of how parameters might be estimated from ringdown data. In what follows, the response of the system is treated as if it is a single harmonic response (i.e. as if the data had been filtered using a modal or bandpass filter); however, in reality there are multiple harmonics. The repercussions of this are that each mode should be investigated separately in order to develop modal parameters, instead of the global parameters deduced from a single harmonic response. For more information on parameter estimation for Iwan elements, refer to (Deaner 2013; Deaner et al. 2013; Sracic, Allen, and Sumali 2012). Another complication in some experimental setups is that there can be multiple sources of damping (such as damping due to bolted joints, due to the support structure, and due to material dissipation), necessitating a specialized technique for decoupling the effects from each type of dissipation (Liang and Feeny 1998). Fortunately for the present analysis, damping due to sources other than

the jointed interface is negligible. Lastly, because jointed systems are very sensitive to a number of parameters (such as bolt torque and loading order, excitation location, interface alignment, etc. (Meyer and Adams 2015)), care needs to be taken in measuring the system to ensure that the variation observed in measured parameters is due to frictional interactions and not setup effects.

Multiple methods have been developed to determine the parameters for a jointed structure, specifically focusing on determining the stiffness and dissipation of the structure as a function of excitation amplitude (Roettgen and Allen Under Review; Kerschen et al. 2006; Kuether and Brake 2016). The application and results of these methods are applied to a set of impact hammer tests conducted on the Brake-Reuß beam (Brake et al. 2014), shown in Fig. 13. The specific experiments reported here are described in (Bonney et al. 2016). The system is suspended by bungee cords to approximate free boundary conditions and is excited via impact hammer and allowed to freely decay. At the interface, the bolts are tightened to 15 Nm, which is representative of realistic joint applications for bolts of this size. In what follows, ring down data is used as it yields oscillatory information at different response (or peak) amplitudes. The mathematical relationships developed here within assume oscillatory behavior.

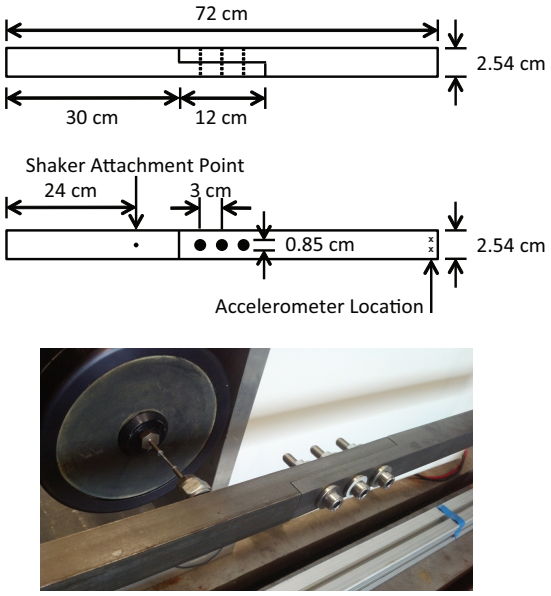

Fig. 13 The geometry of the Brake-Reuß beam.

A typical response for a large amplitude impact is shown in Fig. 14. Due to the lap joint located in the center of the system, the response is dependent upon excitation amplitude. That is, as the response amplitude decreases, the system is expected to stiffen (increase in frequency) due to a transition from macroslip to microslip, and the amount of energy dissipated per oscillation is expected to reduce (again, due to the transition from macroslip to microslip). In these specific experiments, the system is not excited to macroslip since that would plastically damage the system. Consequently, the shift from high amplitudes to

low amplitudes is subtle, but still observable in Fig. 15, which is the unfiltered spectogram of the time history response from Fig. 14.

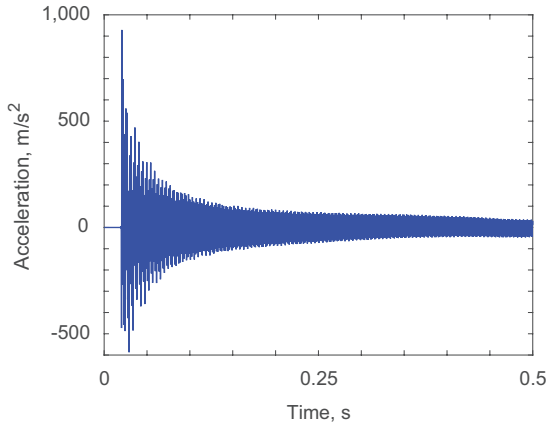

Fig. 14 Representative time history for a large amplitude impulse excitation.

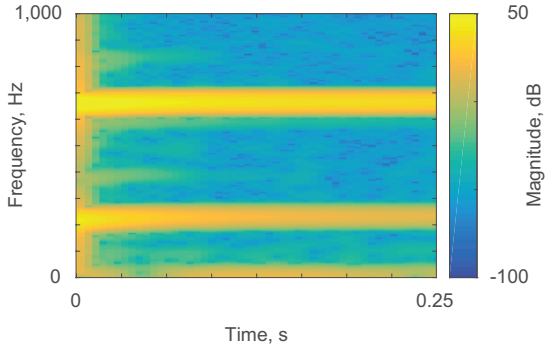

Fig. 15 Spectogram for the time history shown in Fig. 14.

From the ring down data, many approaches are available to extract the stiffness and damping characteristics of the system, including the Hilbert transform (Roettgen and Allen Under Review), wavelet methods (Kerschen et al. 2006), and the short time Fourier transform (STFT) (Kuether and Brake 2016), which is used in the present analysis. In order to deduce the parameters to describe the interface with a RIPP joint, 18 different impact tests are used in which the impact excitation is varied from approximately 100 N to 2000 N. While 18 tests were used, only a subset is needed to deduce a set of parameters for a RIPP joint model; the benefit of 18 tests is in being able to develop a statistical distribution of parameters for the RIPP joint model that describe test-to-test variability. The development of a statistical distribution of parameters if further discussed in (Bonney et al. 2016); here, the derivation of each parameter is discussed in detail as an example of parameter estimation techniques for the RIPP joint model. One important caveat is that in systems with multiple modes in the response, such as the present system, the following techniques are for deriving the modal joint properties (see, for instance, (Deaner et al. 2015; Roettgen et al. 2014)) instead of global joint properties. To do this, the data must first be filtered for the mode of interest.

The stiffness of the system is inferred from the evolution of the primary natural frequency with response amplitude (Fig. 16). For response amplitudes below 4 μm, the natural frequency is con-

stant at approximately 230 Hz. Some noise is observed, though, due to the process of extracting frequency and dissipation data from the impact experiments. At response amplitudes above 4 μm, a significant decrease is observed in the natural frequency such that at an amplitude of 100 μm, the natural frequency is approximately 213 Hz. This change in frequency ($\triangle\omega$) is directly related to K_T as

$$K_T = m \times \triangle\omega^2 \approx 1.1 \times 10^6 \,\mathrm{N/m}. \tag{40}$$

In this calculation, m is the modal mass taken here as 3.67 kg.

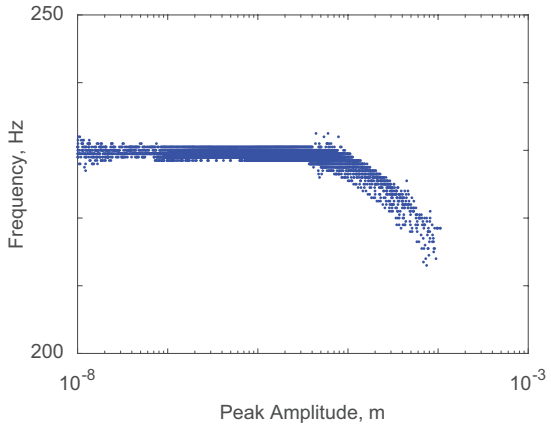

Fig. 16 Frequency versus amplitude data synthesized from 18 different impact tests.

A second quantity that can be discerned from the stiffness plot is ϕ_{MAX}, which is later used to deduce F_S. There are two different methods for approximating ϕ_{MAX}. From (Roettgen and Allen Under Review), ϕ_{MAX} is approximated using data that includes macroslip as the amplitude at which the response frequency is the average of $0.99\omega_1$ and $1.01\omega_2$, where ω_1 is the frequency at very low response amplitudes and ω_2 is the frequency at very large response amplitudes. Here, as macroslip is not observed in the data, ϕ_{MAX} is approximated as ten times the largest response amplitude since the system does not transition to complete macroslip. In this case, $\phi_{MAX} = 2$ mm. The consequence of this approximation is that this parameter is valid for the experiments reported, but 'small' errors are expected to occur for larger excitation amplitudes as no data regarding macroslip is recorded. The term 'small' is used as the model is still expected to be reasonable, but not precise in describing the transition from microslip to macroslip. An alternative approach for characterizing the macroslip properties is highlighted in (Di Maio, Schwingshackl, and Sever 2016), in which modes that have a relatively high engagement of the joint are excited using a response amplitude control method.

One last quantity that is potentially able to be deduced from the frequency data is the pinning stiffness. However, as the system is not excited to macroslip, the pinning stiffness K_P cannot be corroborated via experiments. Instead, as suggested in Section 2.1, the pinning properties are

deduced solely from the material and geometric properties of the system. If the system is excited past macroslip into the pinning regime, the frequency data would exhibit a significant increase in frequency at high response amplitudes that is much greater than the natural frequency at low amplitude responses.

The STFT method also calculates the damping ratio ζ as a function of excitation amplitude. Using the definition of the log decrement

$$\Delta = \frac{2\pi\zeta}{\sqrt{1-\zeta^2}} = \log\left(\frac{x_j}{x_{j+1}}\right), \tag{41}$$

with two adjacent peaks in a decaying transient signal having amplitudes x_j and x_{j+1}, the dissipation per cycle $\mathcal{D}$ is calculated as the difference in energy between the two peaks

$$\mathcal{D} = \frac{1}{2}\omega^2 m u_0^2 \left(\left(e^{2\pi\zeta/\sqrt{1-\zeta^2}}\right)^2 - 1\right), \tag{42}$$

where u_0 is the response amplitude. From (Segalman 2005), $\mathcal{D}$ is directly related to χ by the slope of $\mathcal{D}$ as a function of amplitude on a log-log plot being $3+\chi$. From the dissipation information in Fig. 17, $\chi \approx -0.76$. The features of the plot near the start of each set of data (i.e. at high amplitudes where the dissipation curves have negative slopes) are artifacts of the signal processing techniques. This type of numerical artifact is also observed in Hilbert transformation methods for deducing joint parameters.

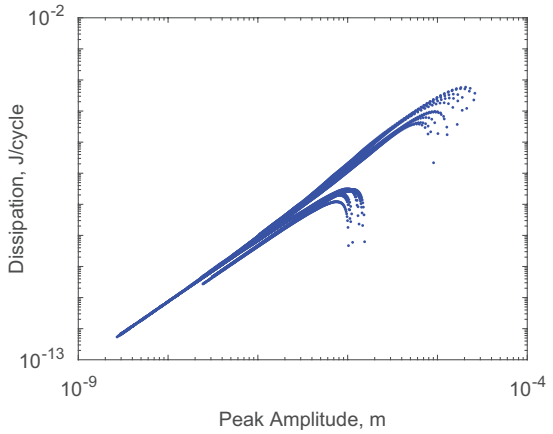

Fig. 17 Calculated energy dissipation curves from 18 different impact tests.

To calculate the remaining two parameters, β and F_S a two step procedure is used. Even though macroslip is not observed in the experiments, the macroslip properties can be inferred from the experiments at low excitation amplitudes. First, F_S is estimated from ϕ_{MAX} as

$$F_S \approx \phi_{MAX} m \omega_\phi^2, \tag{43}$$

with frequency ω_ϕ at the response amplitude equal to ϕ_{MAX} (or largest recorded amplitude when macroslip is not observed). Second, β is calculated using this approximation via (Segalman 2005)

$$\beta = \left(\frac{F_S}{\phi_{MAX} K_T} - \frac{\chi+1}{\chi+2}\right) \Bigg/ \left(1 - \frac{F_S}{\phi_{MAX} K_T}\right). \tag{44}$$

Lastly, F_S is recalculated using this value of β and the dissipation values (Segalman 2005)

$$\mathcal{D} = 4\left(\frac{u_0}{\phi_{MAX}}\right)^{\chi+3}\left(\frac{F_S^2}{K_T}\right) \times\left(\frac{(\beta+1)(\chi+1)}{\left(\beta+\frac{\chi+1}{\chi+2}\right)^2(\chi+2)(\chi+3)}\right), \quad (45)$$

Solving for F_S yields

$$F_S = \left(\left(\frac{\phi_{MAX}}{u_0}\right)^{\chi+3}\frac{\mathcal{D}K_T}{4} \left(\frac{\left(\beta+\frac{\chi+1}{\chi+2}\right)^2(\chi+2)(\chi+3)}{(\beta+1)(\chi+1)}\right)\right)^{1/2}. \quad (46)$$

Equations 45 and 46 assume that the force across the joint F_0 over each period of oscillation is related to the peak displacement

$$\frac{F_0}{F_S} \approx \frac{u_0}{\phi_{MAX}}. \quad (47)$$

As a result, Eq. 46 is valid only for low response amplitudes as the constitutive behavior of the joint at low amplitudes is dominated by the tangential stiffness K_T (whereas at higher amplitudes, softening is observed as portions of the interface begin to slip, see Fig. 3), as shown in Fig. 18. Thus, the macroslip properties are deduced from the response in the microslip regime. Both F_S and β are iteratively calculated until the initial estimate for F_S agrees with the calculation of Eq. 46. Each of the parameters deduced from the experiments reported in (Bonney et al. 2016) are summarized in Table 2.

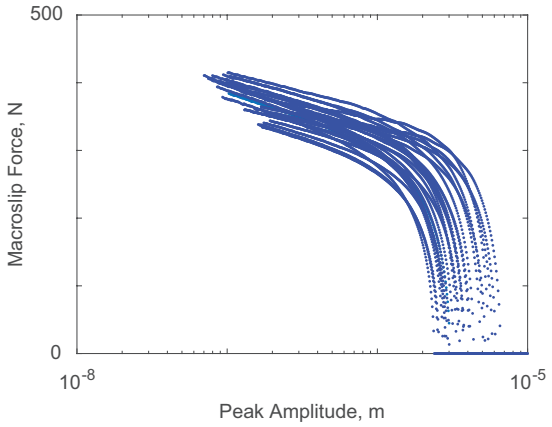

Fig. 18 Calculated macroslip force value from low amplitude impact tests.

Property	Value
Tangential Stiffness, K_T	1.1×10^6 N/m
Macroslip Displacement, ϕ_{MAX}	2 mm
Macroslip Force, F_S	400 N
Dissipation Exponent, χ	-0.76
Stiffness Ratio, β	0.16
Pinning Stiffness, K_P	10^7 N/m
Pinning Clearance, δ_P	2 mm

Table 2 Joint parameters deduced from the experiments of (Bonney et al. 2016).

5 Summary

The analytical representation of the discretized Iwan model is formulated in this research for several different friction models: the four-parameter distribution of Segalman, the five-parameter extension of Segalman's model by Mignolet, and the uniform distribution originally used by Iwan. The analytical model is further extended to consider an

Iwan-Stribeck model in order to demonstrate how to extend the model to more complicated functional forms, and discussion of how to extend the model to other distributions is also presented. The advantage of an analytical representation of the Iwan model is a dramatic improvement in computational time compared to the discretized Iwan model developed in (Segalman 2005). The key hypothesis that enables the analytical formulation is that on a load reversal, there is a new distribution of sliders in sticking and slipping states that resembles a scaled version of the original distribution of sliders. Two examples are provided to highlight features of the model: a transient response to a sinusoidal force, and a parameter extraction from impact data reported for the Brake-Reuß beam in (Bonney et al. 2016).

Acknowledgements

The author would like to thank Rob Kuether, Caroline Nielsen, and Scott Smith for their development of the STFT algorithms used in the examples.

References

Armstrong-Hélouvry, B., P. Dupont, and C. Canudas de Wit (1994). "A Survey of Models, Analysis Tools and Compensation Methods for the Control of Machines with Friction". In: *Automatica* 30, pp. 1083–1138.

Bauschinger, J. (1886). "On the Change of Position of the Elastic Limit of Iron and Steel Under Cyclic Variations of Stress". In: *Mitteilung Mechanisch-Technischen Laboratoriums in München* 13, pp. 1–115.

Bonney, M. S. et al. (2016). "Experimental Determination of Frictional Interface Models". In: *34t International Modal Analysis Conference (IMAC XXXIV)*. Orlando, FL.

Brake, M. R. (2014). "The Role of Epistemic Uncertainty of Contact Models in the Design and Optimization of Mechanical Systems with Aleatoric Uncertainty". In: *Nonlinear Dynamics* 77, pp. 899–922.

Brake, M. R. et al. (2014). "Variability and Repeatability of Jointed Structures with Frictional Interfaces". In: *32nd International Modal Analysis Conference (IMAC XXXII)*. Orlando, FL.

Cigeroglu, E., N. An, and C.-H. Menq (2007). "A Microslip Friction Model with Normal Load Variation Induced by Normal Motion". In: *Nonlinear Dynamics* 50, pp. 609–626.

Deaner, B. (2013). *Modeling the Nonlinear Damping of Jointed Structures Using Modal Models.*

Masters Dissertation. University of Wisconsin-Madison, Madison, WI.

Deaner, B. J. et al. (2013). "Investigation of Modal Iwan Models for Structures with Bolted Joints". In: *31st International Modal Analysis Conference (IMAC XXXI)*. Garden Grove, CA.

Deaner, B. J. et al. (2015). "Application of Viscous and Iwan Modal Damping Models to Experimental Measurements From Bolted Structures". In: *ASME Journal of Vibration and Acoustics* 137, p. 021012.

Deckstein, D. and G. Traufetter (2012). "Weight Loss for Superjumbos: The A380 and the Aviation Engineering Dilemma". In: *Der Spiegel*.

Di Maio, D., C. Schwingshackl, and I. A. Sever (2016). "Development of a Test Planning Methodology for Performing Experimental Model Validation of Bolted Flanges". In: *Nonlinear Dynamics* 83, pp. 983–1002.

Gaul, L. and R. Nitsche (2000). "Friction Control for Vibration Suppression". In: *Mechanical Systems and Signal Processing* 14, pp. 139–150.

— (2001). "The Role of Friction in Mechanical Joints". In: *ASME Applied Mechanics Reviews* 54, pp. 93–110.

Ishlinskii, A. Y. (1944). "Some Applications of Statistical Methods to Describing Deformations of Bodies". In: *Izvestiya Akademii Nauk SSSR* 9, pp. 580–590.

Iwan, W. D. (1966). "A Distributed-Element Model for Hysteresis and its Steady State Dynamic Response". In: *ASME Journal of Applied Mechanics* 33, pp. 893–900.

— (1967). "On a Class of Models for the Yielding Behavior of Continuous and Composite Systems". In: *ASME Journal of Applied Mechanics* 34, pp. 612–617.

Jayakumar, P. (1987). *Modeling and Identification in Structural Dynamics*. Doctoral Dissertation. California Institute of Technology, Pasadena, CA.

Jenkins, G. M. (1962). "Analysis of the Stress-Strain Relationships in Reactor Grade Graphite". In: *British Journal of Applied Physics* 13, pp. 30–32.

Johnson, K. L. (1985). *Contact Mechanics*. Cambridge: Cambridge University Press.

Kerschen, G. et al. (2006). "Past, Present and Future of Nonlinear System Identification in Structural Dynamics". In: *Mechanical Systems and Signal Processing* 20, pp. 505–592.

Kuether, R. J. and M. R. W. Brake (2016). "Instantaneous Frequency and Damping from Transient Ring-Down Data". In: *34t International*

Modal Analysis Conference (IMAC XXXIV). Orlando, FL.

Liang, J. W. and B. F. Feeny (1998). "Identifying Coulomb and Viscous Friction from Free-Vibration Decrements". In: *Nonlinear Dynamics* 16, pp. 337–347.

Masing, G. (1926). "Self-Stretching and Hardening for Brass". In: *Proceedings of the Second International Congress for Applied Mechanics*, pp. 332–335.

Meyer, J. J. and D. E. Adams (2015). "Theoretical and Experimental Evidence for Using Impact Modulation to Assess Bolted Joints". In: *Nonlinear Dynamics* 81, pp. 103–117.

Petrov, E. P. and D. J. Ewins (2004). "Generic Friction Models for Time-Domain Vibration Analysis of Bladed Disks". In: *ASME Journal of Turbomachinery* 126, pp. 184–192.

Prandtl, L. (1928). "Ein Gedankenmodell zur kinetischen Theorie der festen Korper". In: *Zeitschrift fur Angewandte Mathematik und Mechanik* 8, pp. 85–106.

Roettgen, D. R. and M. S. Allen (Under Review). "Nonlinear Characterization of a Bolted, Industrial Structure Using a Modal Framework". In: *Mechanical Systems and Signal Processing*.

Roettgen, D. R. et al. (2014). "Feasibility of Describing Joint Nonlinearity in Exhaust Components with Modal Iwan Models". In: *ASME International Design Engineering Technical Conferences IDETC/CIE*. Buffalo, NY.

Segalman, D. J. (2005). "A Four-Parameter Iwan Model for Lap-Type Joints". In: *ASME Journal of Applied Mechanics* 72, pp. 752–760.

Segalman, D. J. and M. J. Starr (2004). *Relationships Among Certain Joint Constitutive Models*. Technical Report SAND2004-4321. Sandia National Laboratories, Albuquerque, NM.

Segalman, D. J. et al. (2009). *Handbook on Dynamics of Jointed Structures*. Technical Report SAND2009-4164. Sandia National Laboratories, Albuquerque, NM.

Smallwood, D. O., D. L. Gregory, and R. G. Coleman (2001). "A Three Parameter Constitutive Model for a Joint which Exhibits a Power Law Relationship Between Energy Loss and Relative Displacement". In: *72nd Shock and Vibration Symposium*. Destin, FL.

Sracic, M. W., M. S. Allen, and H. Sumali (2012). "Identifying the Modal Properties of Nonlinear Structures Using Measured Free Response Time Histories from a Scanning Laser Doppler

Vibrometer". In: *30th International Modal Analysis Conference (IMAC XXX)*. Jacksonville, FL.

Van de Vrande, B. L., D. H. Van Campen, and A. de Kraker (1999). "An Approximate Analysis of Dry-Friction-Induced Stick-Slip Vibrations by a Smoothing Procedure". In: *Nonlinear Dynamics* 19, pp. 157–169.

Wang, X. Q. and M. P. Mignolet (2014). "Stochastic Iwan-Type Model of a Bolted Joint: Formulation and Identification". In: *32nd International Modal Analysis Conference (IMAC XXXII)*. Orlando, FL.